CHEMISTRY
A EUROPEAN JOURNAL

DOI: 10.1002/chem.200600032

Metal-Particle-Induced, Highly Localized Site-Specific Etching of Si and Formation of Single-Crystalline Si Nanowires in Aqueous Fluoride Solution

Kuiqing Peng,*[a, b, c] Hui Fang,[a] Juejun Hu,[a] Yin Wu,[a] Jing Zhu,*[a] Yunjie Yan,[a] and ShuitTong Lee[b]

Abstract: A straightforward metal-particle-induced, highly localized site-specific corrosion-like mechanism was proposed for the formation of aligned silicon-nanowire arrays on silicon in aqueous HF/$AgNO_3$ solution on the basis of convincing experimental results. The etching process features weak dependence on the doping of the silicon wafers and, thus, provides an efficient method to prepare silicon nanowires with desirable doping characteristics. The novel electrochemical properties between silicon and active noble metals should be useful for preparing novel silicon nanostructures and also new optoelectronic devices.

Keywords: electrochemistry · etching · metal ions · semiconductors · silicon nanowires

Introduction

One-dimensional semiconductor nanostructures have proven to be good candidates for novel nanoscale optoelectronics and ultrasensitive, miniaturized molecule sensors.[1] As a special form of crystalline silicon, silicon nanowires (SiNWs) have attracted much interest due to their unusual quantum-confinement effects as well as their potential application in optoelectronics and other devices.[2] SiNW-based nanoelectronic devices with quantization results have been demonstrated.[3] SiNWs have also been applied to highly sensitive biological and chemical sensors by exploiting their extremely high sensitivity to conductance.[4] Recently, two main fabrication technologies have been proposed for SiNWs. The first one is top-down approach, based on silicon-wafer processing by means of high-resolution lithography and dry or wet etching.[5] The conventional lithography techniques offer greater flexibility and precision in device positioning; however, the fabrication of silicon nanowires with high-aspect ratio still has remained a challenge to conventional lithography. The second technique is a bottom-up technique, based on the well-known vapor-liquid-solid (VLS) growth of nanowires by means of chemical-vapour deposition (CVD) with SiH_4 (or $SiCl_4$) as precursor and Au nanoparticles as catalysts.[6] The size of the catalyst nanoparticle determines the diameter of the nanowire grown. Recently, Yang et al. demonstrated that vertically aligned single-crystalline silicon nanowires with controlled dimensions and specific placement could be produced on silicon substrate by using directed colloid seeding for the conventional VLS-CVD method.[7] The vertically aligned growth of SiNWs makes this process ideal for fabricating array devices, such as variable field effect transistor (VFET) circuits and two-dimensional photonic crystals.

Silicon exhibits novel electrochemical properties in solutions containing hydrofluoric acid, and the complex electrochemical etching behavior has raised considerable research interest.[8] By utilizing the novel electrochemical behavior of silicon in hydrofluoric acid, various silicon nanostructures, such as luminescent porous silicon and silicon nanowires, have been prepared.[9] Large-area vertically aligned silicon nanowires could be readily produced on a silicon wafer by immersing cleaned silicon into aqueous HF solution containing noble-metal ions for an appropriate time.[10] The fabrication process is rather simple and rapid, compared with previously reported VLS and oxide-assisted growth (OAG) methods.[11,12] After the treatment, the etched silicon sub-

[a] Dr. K. Q. Peng, H. Fang, J. J. Hu, Y. Wu, Prof. J. Zhu, Y. J. Yan
Laboratory of Advanced Materials
Department of Materials Sciences and Engineering
Tsinghua University, Beijing, 100084 (P. R. China)
Fax: (+86) 10-6277-2507
E-mail: kuiqing99@mails.tsinghua.edu.cn
jzhu@mail.tsinghua.edu.cn

[b] Dr. K. Q. Peng, Prof. S. T. Lee
Center of Super-Diamond and Advanced Films (COSDAF)
City University of Hong Kong, Hong Kong SAR (China)

[c] Dr. K. Q. Peng
Department of Materials Science and Engineering
Beijing Normal University, Beijing, 100875 (China)

WILEY InterScience DISCOVER SOMETHING GREAT
© 2006 Wiley-VCH Verlag GmbH & Co. KGaA, Weinheim

strates were wrapped with thick silver dendritic film. Large-area vertically aligned silicon nanowires could be observed on silicon substrates after peeling off the silver dendritic film. Owing to the strong galvanic displacement reaction between silicon and highly reactive HF/$AgNO_3$ solution, the etched silicon wafer was always wrapped in a thick layer of silver dendritic film, which significantly precludes the exploration of the intrinsic etching mechanism of silicon in HF/$AgNO_3$ solution. Because there is insufficient experimental evidence to support it, the tentative dendrite-assisted self-assembled nanoelectrochemistry mechanism is not convincing. We recently found that large-area, one-dimensional Si-nanostructure arrays could be prepared on silicon wafers by metal-particle catalytic etching in aqueous HF/$Fe(NO_3)_3$ solution; no metal deposition occurs during the production of one-dimensional Si nanostructures; this prompted us to survey the mechanism proposed for SiNWs in aqueous HF/$AgNO_3$ solution again. We systemically investigated the morphological evolution of silicon wafers in HF/$AgNO_3$ solution. Here, we present our new position regarding the etching process of Si wafers in aqueous HF/$AgNO_3$ solution by combining results of new experiments and previous knowledge. A metal-particle-induced, localized, and strongly enhanced catalytic oxidation and dissolution of Si substrates is proposed to explain the formation process of silicon nanowires in aqueous HF/$AgNO_3$ solution.

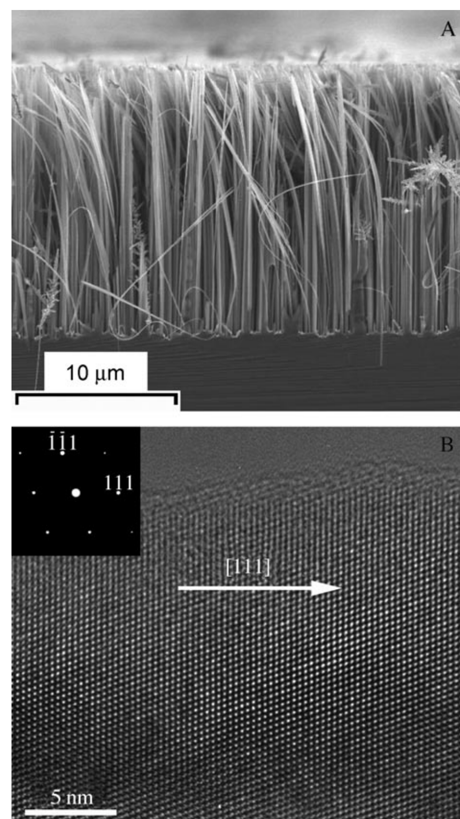

Figure 1. A) TEM image showing a cross-sectional view of SiNW arrays on an etched silicon wafer; B) HRTEM image of a single silicon nanowire and its selected-area electron diffraction pattern (insert).

Results and Discussion

High-quality Si nanowire arrays can be produced on the Si wafer by simply immersing the wafer into HF/$AgNO_3$ solution for an appropriate etching time. Figure 1A shows the vertically well-aligned large-area nanowire array formed on a p-type (111) Si wafer at 50 °C for 1 h; the etching solution contains 4.6 M^{-1} HF and 0.01 M^{-1} silver nitrate. Figure 1B shows a high-resolution transmission electron microscopy (HRTEM) image of a single nanowire carefully removed from the Si substrate. The selected-area electron diffraction (SAED) pattern in the inset of Figure 1B and its corresponding fast Fourier transform (FFT) pattern demonstrate its single-crystal nature and the [111] axial crystallographic orientation, which is the same as the orientation of the used Si wafer. Silicon nanowires with [100] axial crystallographic orientation could be readily obtained by etching the Si wafer with (100) orientation. SiNWs with controllable [100] direction are of particular interest in optoelectronic applications due to the stronger direct nature of light emission in the visible regime relative to nanowires grown along [111] and [112]. In contrast, for the traditional VLS-based growth techniques, SiNWs commonly grow in the [111] and [112] direction, and rarely in [100] direction.

The formation mechanism of the as-prepared silicon nanowires is quite different from previously proposed mechanisms for silicon nanowires, such as VLS and the oxide-assisted growth mechanism.[10,11] The production of SiNWs on a Si wafer in HF/$AgNO_3$ solution should be the result of selective etching. However, why and how does the selective etching occur? How does the etching interface propagate during etching? To answer these questions, the kinetic etching process of Si in HF/$AgNO_3$ solution should be studied carefully. However, due to the intense galvanic displacement reaction, the large quantities of silver dendrites produced would closely wrap the etched Si wafer. Thus, the surface morphology of the etched Si wafer cannot be readily accessible, not to mention the etching mechanism. However, the surface morphology of the Si wafer at the early stage in the HF/$AgNO_3$ solution can be revealed and may give us some idea of the etching process. Therefore, we carefully investigated the incipient temporal evolution of the etching morphology of Si wafer in aqueous HF/$AgNO_3$ solution. Figure 2 shows the top view of p-type (111) Si wafers etched in HF/$AgNO_3$ solution at different times. The etching solution contains 4.6 M^{-1} HF and 0.02 M^{-1} silver nitrate. According to the galvanic displacement reaction, silicon etching and silver deposition occur simultaneously at the silicon surface. At the initial stage, for example, after 30 s (Figure 2A), a high density of precipitated Ag particles could be seen on the etched Si surface, whereas no corresponding Si microstructures were observed on the surface. We also noted that the Ag deposits on the n-type silicon wafer have a higher distribution density than on the p-type silicon wafer, but the Ag deposits on the p-type silicon wafer are larger. We sug-

 © 2006 Wiley-VCH Verlag GmbH & Co. KGaA, Weinheim

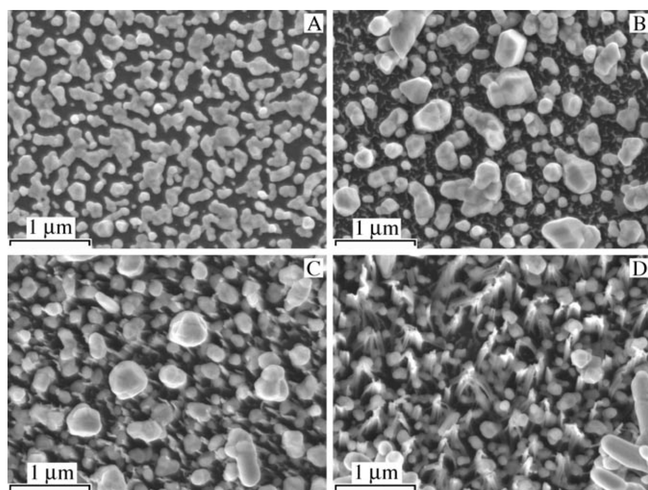

Figure 2. TEM images showing top views of p-type (111) Si wafers etched in HF/$AgNO_3$ solution for A) 30 s, B) 1 min, C) 5 min, and D) 10 min.

gest that the differences could be attributed to the higher surface-electron concentration of n-type silicon and also the difference in hole concentration at the silicon/solution interface. As the etching time increases, Si microstructures gradually become apparent in the space between the Ag particles; simultaneously, some silver particles grow into larger particles. After 5 min or more, many nanometer-sized, needle-shaped Si microstructures protrude outward from the spaces between Ag particles on the silicon surface (Figure 2C and D). These phenomena imply that the appearance of Si needles may be ascribed to the sinking of Ag particles into bulk silicon, because "growth" of Si needles is impossible in this case. Large silver particles would grow into branched dendrites if the etching time is prolonged further. A fraction of the Si surface was covered with silver dendrites after 5 min; a majority of the Si surfaces were covered with silver dendrites after 10 min. After 30 min or more, the entire etched Si wafer was closely wrapped in thick silver dendrites. Large-area silicon-nanowire arrays could be observed after peeling off the silver dendritic film.

To clarify the behavior of Ag deposits during silicon etching, we performed a detailed cross-sectional morphology investigation of the etched Si wafer in aqueous HF/$AgNO_3$ solution. The cross-section specimens were prepared by mechanically cleaving the etched Si wafers. The covered silver dendritic films were not removed, to avoid unexpected effects on the cross-section morphology before the preparation of cross-section specimens. Figure 3A shows the cross-sectional view of a p-type (111) Si wafer etched in HF/$AgNO_3$ solution for 5 min. The Si needles in between the Ag particles are about 500 nm long and are vertically aligned on the surface of the etched Si wafer. Results of our detailed experiments confirmed that similar vertically aligned Si needles could be produced on Si wafers with other orientations, such as (100) and (110). This characteristic can be employed to control the axial orientation of nanowires by choosing substrates with corresponding orientations.

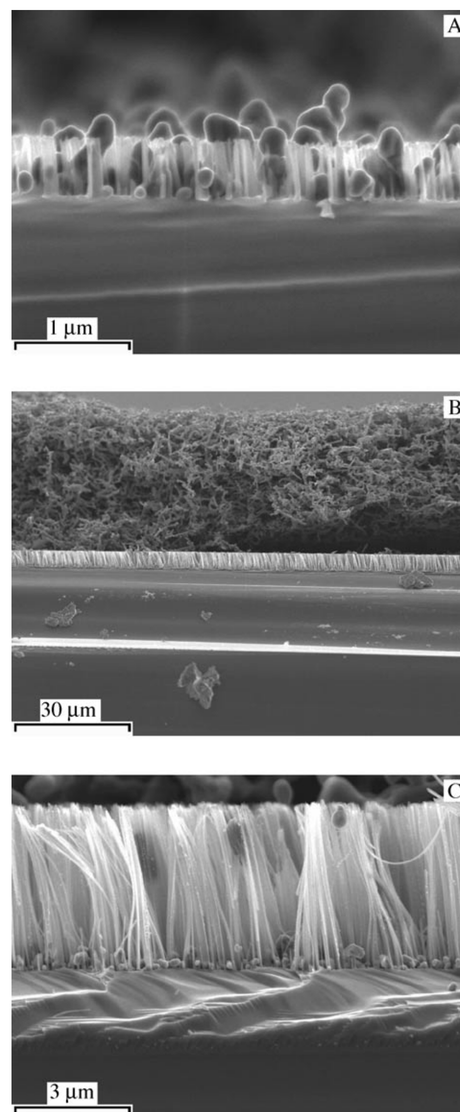

Figure 3. TEM images showing cross-sectional views of p-type (111) Si wafers etched in HF/$AgNO_3$ solution for A) 5 min and B,C) 30 min.

In Figure 3B, the wafer etched in HF/$AgNO_3$ solution for 30 min is covered with a Ag dendritic film with a thickness of about 40 μm. Under the silver dendritic film, vertically aligned long SiNWs can be seen. These SiNWs are about 4 μm long (Figure 3C). In this high-magnification SEM image, many silver particles can be observed at the bottom of the SiNW forest and are located among vertically aligned SiNWs. The sizes of these particles are very close to the size of silver particles deposited at the initial etching stage. This indicates that these Ag particles experience no significant growth in size during the etching process, although some other Ag particles have grown into very large ramified dendrites. As etching time increases, longer vertically aligned SiNWs are created on the silicon surface. Therefore, the length of SiNWs can be readily controlled by adjusting the etching time in HF/$AgNO_3$ solution.

© 2006 Wiley-VCH Verlag GmbH & Co. KGaA, Weinheim

Notably, these experimental results indicate that no Si nanowires are capped with Ag particles, as suggested in previous mechanisms. In contrast, the Ag particles are located among the ends of vertically aligned Si nanowires. These results strongly challenge the rationality of a previously proposed mechanism, which lacks the support of experimental evidence. By combining these observations with the electrochemistry of the Si/solution interface, we present a simplified quantitative model for the growth mechanism of SiNWs in aqueous $HF/AgNO_3$ solution. Figure 4 shows the schematic formation of vertically aligned Si nanowires on a Si wafer in aqueous $HF/AgNO_3$ solution.

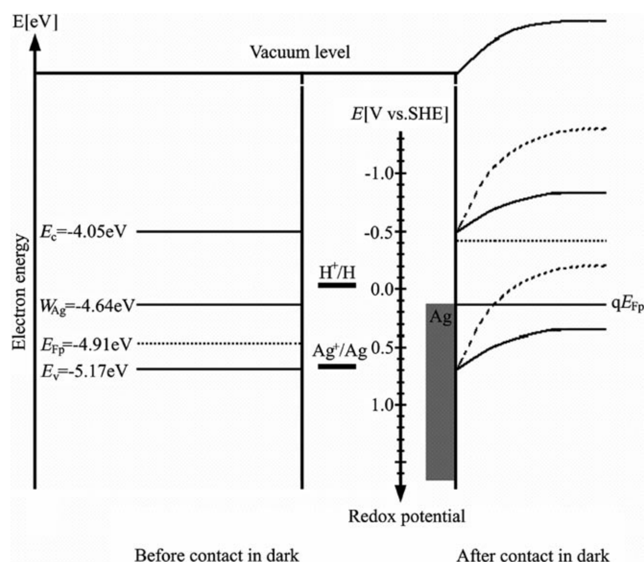

Figure 4. Energy-band diagrams for p-type Si in aqueous $HF/AgNO_3$ solution. Left: Before contact in the dark; typical values for energy levels are shown referenced to vacuum and to SHE. Right: After contact in the dark; energy-band bending of silicon and the formation of quasi-Schottky Ag/Si interface. qE_{Fp} denotes the quasi-Fermi level at the interface.

Electroless silver deposition (EMD) on a silicon surface from $HF/AgNO_3$ solution is based on the galvanic displacement reaction, in which two simultaneous processes occur at the silicon surface: the cathodic reaction (hydrogen evolution [Eq. (1)] or reduction of Ag^+ ions [Eq. (2)], which produces metallic Ag deposits) and the anodic reaction (oxidation of silicon, either an electron-releasing [Eq. (3)] or hole-consuming [Eq. (4)] type of reaction), during which the charges released by the oxidation of silicon atoms are transferred to the sites of silver deposition (SHE = standard hydrogen electrode):

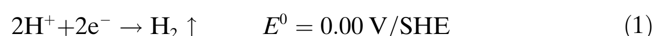

$$2H^+ + 2e^- \rightarrow H_2\uparrow \qquad E^0 = 0.00\ \text{V/SHE} \tag{1}$$

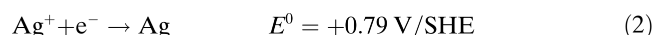

$$Ag^+ + e^- \rightarrow Ag \qquad E^0 = +0.79\ \text{V/SHE} \tag{2}$$

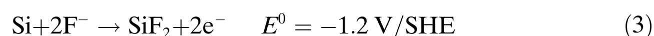

$$Si + 2F^- \rightarrow SiF_2 + 2e^- \qquad E^0 = -1.2\ \text{V/SHE} \tag{3}$$

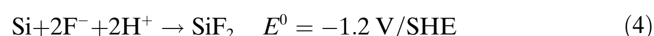

$$Si + 2F^- + 2H^+ \rightarrow SiF_2 \qquad E^0 = -1.2\ \text{V/SHE} \tag{4}$$

The driving force of the charge exchange is the difference between the redox potentials of the redox species in solution and the Fermi level of silicon. The redox potential at equilibrium of each electrochemical reaction [Eqs. (1)–(4)] could be calculated approximately by using the Nernst relationship [Eqs. (5)–(7)] as follows:

$$E_{H}\ (\text{V/SHE}) = 0.00 + \frac{RT}{F}\ln[H^+] \tag{5}$$

$$E_{Ag}\ (\text{V/SHE}) = 0.80 + \frac{RT}{F}\ln[Ag^+] \tag{6}$$

$$E_{Si}\ (\text{V/SHE}) = -1.20 - \frac{RT}{F}\ln[F^-] \tag{7}$$

in which E is equilibrium potential, R is the ideal-gas constant $8.314\ \text{J K}^{-1}\text{mol}^{-1}$, F is the Faraday constant $96500\ \text{C mol}^{-1}$, T is the absolute temperature, and $[H^+]$ and $[Ag^+]$ are the molarities of H^+ and Ag^+ ions in HF solution, respectively. The dissociation constant of hydrofluoric acid is assumed to be about $K_1 = 6.8\times10^{-4}$ at approximately room temperature. Thus, the concentration of hydrogen ions was calculated to be around 5.558×10^{-2} M. We can then obtain the equilibrium potentials of $E_{si} = 1.081$ V and $E_H = -0.008$ V (-4.42 eV). In HF solution, if the Ag^+ concentration is assumed to be 0.01 M, the equilibrium potential of E_{Ag} is about 0.661 V (-5.161 eV).

Figure 4 is a simplified energy-band diagram for the interface between Si and HF solution containing Ag^+ ions. It shows the energetics of the reduction of Ag^+ ions and electron transfer at the silicon/solution interface. The redox potentials of the reducible species indicated in the diagram are expressed with respect to a value of -4.50 eV for the standard hydrogen electrode (SHE). The Fermi level of silicon and the redox potential of the redox species in solution tended to align as silicon was immersed into the solution. For p-type silicon with no Ag^+ present in HF solution, the Fermi level of silicon ($E_{Fp} = -4.91$ eV) is lower than the redox potential of $E_{H+/H} = -4.42$ eV. The silicon surface would be depleted of majority carriers (holes); and both the conduction and valence bonds would bend downwards. Upon addition of Ag^+ to the HF solution, the band bending would be less.

The energy diagrams shown in Figure 4 indicate that the bonding electrons of surface silicon atoms can be transferred to Ag^+ ions in aqueous HF solution; that is, in the Ag^+/Ag redox system with energy levels strongly overlapping with the valence bond of silicon, hole injection becomes more likely and the reduction of Ag^+ ions is not limited by the concentration of minority carriers. Such charge transfer constitutes the corrosion current flowing from the local cathodic sites to anodic sites, and results in the deposition of silver atoms on the cathodic sites of silicon surface and also the dissolution of surface silicon atoms. The anodic oxidation of silicon dissolution should occur in the close vicinity of Ag nuclei to realize direct electron transport.

 © 2006 Wiley-VCH Verlag GmbH & Co. KGaA, Weinheim

As soon as Ag deposition begins, Ag^+ ions in the vicinity of the silicon surface capture electrons from the valence band of Si and are deposited in the form of nanoscale metallic Ag nuclei. The Ag nuclei adhering to the silicon surface have higher electronegativity than Si and, therefore, strongly attract electrons from Si to become negatively charged (Figure 5A). These Ag nuclei have strong catalytic activity for the cathodic reaction and could provide a catalytc surface for the cathodic reaction (reduction of Ag ions). Therefore, the subsequent dynamic reduction process of Ag^+ ions would be greatly influenced. That is, the Ag^+ ions approaching the silicon surface would be reduced preferentially on initial Ag nuclei sites rather than on bare silicon, whereas the electrons are transferred through the Ag/Si interface. Notably, the present Ag/Si Schottky interface is different from the usual stable Ag/Si Schottky interface because the simultaneous dissolution of silicon would result in the degradation of the electronic properties of the quasi-Schottky Ag/Si interface. Due to the relatively low-energy barrier for holes in the Ag/Si interface, electrons can be transferred from the Ag nuclei to Ag^+ ions in solution by hole injection through the quasi-Schottky Ag/Si interface (Figure 5A).

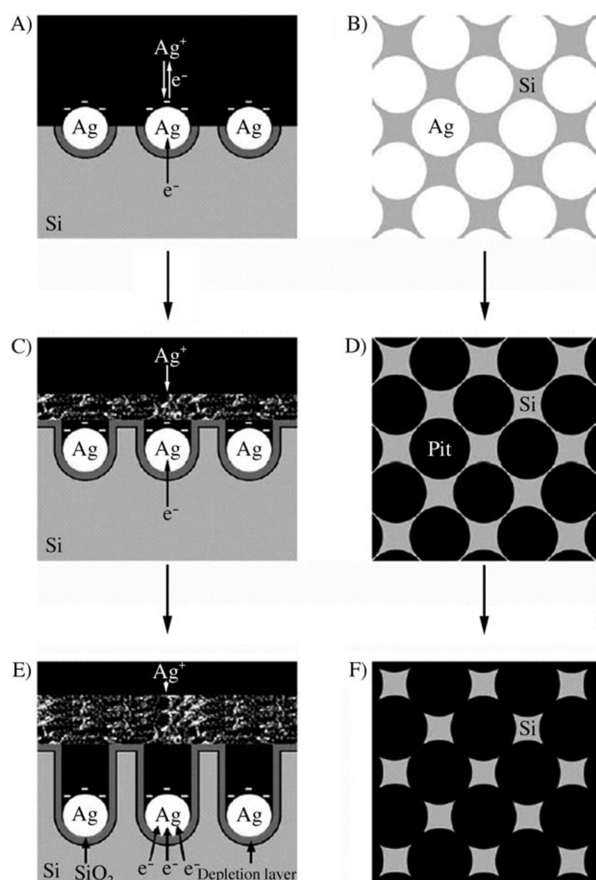

Figure 5. Schematic representation of the formation of vertically aligned SiNW arrays on a Si surface in aqueous $HF/AgNO_3$ solution; A→C→E follows the lateral view of the etching process; B→D→F follows the top view of etching process.

Therefore, the Fermi energies tend to align throughout the Si/Ag/solution interface under these conditions; and the present deposition of Ag leads to the growth of silver nuclei by metal-on-metal deposition. Thus, the initially dense Ag nuclei would grow into large particles on the silicon surface as deposition time increases. Simultaneously, because the Si underneath the Ag particles releases as many electrons as are required by the Ag ions to be reduced, localized excess oxidation would occur underneath these Ag particles. Shallow pits would immediately form underneath these Ag particles, due to the etching away of the SiO_2 produced. Consequently, the pits eventually contain the Ag particles that are responsible for making them (Figure 5A). This similar metal-induced pit formation was reported previously by Morinaga, Kim, and Mitsugi in their study of electrochemical copper deposition in dilute hydrofluoric acid (DHF) solution.[13] These metal particles were trapped in the resulting pits and could not move horizontally. Our SEM observations also confirm this metal-induced pitting phenomena.

As reaction time increases, some suitably small Ag particles would sink further into the deepened pits, whereas larger Ag particles that could not enter the pits would grow into large, branched silver dendrites that eventually cover the whole surface of the Si wafer (Figure 5C). Thus, the subsequent deposition of Ag would occur on these silver dendrites, whose growth consumes large quantities of superfluous, silver atoms. This effectively prevents the formation of a compact Ag granule film and also the growth of small Ag particles trapped in the pits. Because the Ag particles are trapped by the pits and cannot move horizontally on the silicon surface, highly localized and site-specific etching would occur underneath these trapped Ag particles. Under these circumstances, the initial shallow pits would deepen as the underlying SiO_2 dissolves and the Ag particles sink further. The deep pits are similar to the nanoholes reported by Tsujino.[14] As the silicon dissolves and Ag ions are reduced, a charge-depletion layer with high resistance would emerge around the Ag particles. The charge-exchange and -transport between anode (Si) and cathode sites (Ag particles) would be more favorable at the Ag/Si interface than at the pore wall: one reason for this is the low-energy barrier for holes in the Ag/Si interface, the other is the shortest charge-transport distance and unique catalytic property of Ag particles for the cathodic reaction. Consequently, oxidation and dissolution of silicon occur at the pore tips (the Ag/Si interface) rather than at the pore walls. Therefore, straight, non-interacting cylindrical pores that run perpendicular to the Si surface would be ultimately produced (Figure 5E); the pore sizes and their separation depend upon the sizes and the areal density of the trapped Ag particles located at the bottom of the deep pores. The subsequent chemical dissolution of thin pore walls would enlarge the pores and lead to merging of nearest-neighbor pores. Finally, after sufficient etching time, a high density of one-dimensional Si nanowires would remain on the silicon surface (Figure 5F). The mecha-

© 2006 Wiley-VCH Verlag GmbH & Co. KGaA, Weinheim

nism proposed here is very similar to that proposed by L. T. Canham for silicon quantum wires.[15]

Furthermore, large-area SiNW arrays also could be produced on a silicon surface in HF/K[$AuCl_4$] solution. We suggest that the etching mechanism is the same as that for Si in HF/$AgNO_3$ solution. In the cases of Si in HF/K_2[$PtCl_6$] or HF/$Cu(NO_3)_2$ solution, the Si surface is covered with a compact Pt- or Cu-granule film that prevents the oxidized silicon ions from penetrating the compact metal film to enter solution. This obstructs the galvanic displacement reaction. Therefore, no similar SiNWs could be generated in either case.

Conclusion

We have restudied the etching behavior of silicon in aqueous fluoride solution that contains noble-metal ions by performing rigorous experimental procedures. The detailed temporal morphological evolution of silicon in HF/$AgNO_3$ solution was investigated. A straightforward metal-induced, highly localized site-specific corrosion-like mechanism was found for the formation of SiNWs on silicon from HF solution. A high density of stable metal particles and silver dendrites on the silicon surface facilitates the final formation of vertically aligned SiNW arrays. The novel electrochemical properties of the interaction between silicon and active noble metals are expected to be useful for preparing novel silicon nanostructures and also new optoelectronic devices.

Experimental Section

The fabrication process involved two main steps: 1) cleaning of the original silicon substrates, 2) immersion of the cleaned silicon substrates into HF-based aqueous solution containing silver nitrate in sealed vessels and treatment for the desired time. The concentrations of the HF and $AgNO_3$ solutions were 4.6 and 0.02 M^{-1}, respectively. After treatment, the etched silicon substrates were wrapped with thick silver dendritic film. Large-area vertically aligned SiNWs could be observed on silicon substrates after peeling off the silver dendritic film. The as-synthesized samples were studied by using a scanning electron microscope (SEM JEOL 6301F and Philips XL 30 FEG) and transmission electron microscope (TEM JEOL 2010F) equipped with an energy-dispersive X-ray spectrometer and a Gatan GIF system. To prepare a TEM specimen the sample was scraped by using a knife, the scraping was collected and was then suspended in ethanol. A drop of this suspension was placed on a carbon copper grid and examined by using a JEOL 2010F microscope.

Acknowledgements

This work was supported by the National Natural Science Foundation, National 973 Project of the People's Republic of China, and 985 Project of Tsinghua University.

[1] a) M. Law, J. Goldberger, P. D. Yang, *Annu. Rev. Mater. Res.* **2004**, *34*, 83; b) X. F. Duan, Y. Huang, R. Agarwal, C. M. Lieber, *Nature* **2003**, *421*, 241; c) M. H. Huang, S. Mao, H. Feick, H. Q. Yan, Y. Y. Wu, H. Kind, E. Weber, R. Russo, P. D. Yang, *Science* **2001**, *292*, 1897; d) Y. Huang, X. F. Duan, C. M. Lieber, *Small* **2005**, *1*, 142; e) M. Law, D. J. Sirbuly, J. C. Johnson, J. Goldberger, R. J. Saykally, P. D. Yang, *Science* **2004**, *305*, 1269.

[2] a) X. Y. Zhao, C. M. Wei, L. Yang, M. Y. Chou, *Phys. Rev. Lett.* **2004**, *92*, 236805; b) D. D. D. Ma, C. S. Lee, F. C. K. Au, S. Y. Tong, S. T. Lee, *Science* **2003**, *299*, 1874; c) D. Y. Li, Y. Y. Wu, P. Kim, L. Shi, P. D. Yang, *Appl. Phys. Lett.* **2003**, *83*, 2934; d) Y. Cui, C. M. Lieber, *Science* **2001**, *291*, 851; e) K. Q. Peng, Z. P. Huang, J. Zhu, *Adv. Mater.* **2004**, *16*, 73; f) K. Q. Peng, Y. Xu, Y. Wu, Y. J. Yan, S. T. Lee, J. Zhu, *Small* **2005**, *1*, 1062.

[3] Y. Cui, C. M. Lieber, *Science* **2001**, *291*, 851.

[4] a) Y. Cui, Q. Wei, H. Park, C. M. Lieber, *Science* **2001**, *293*, 1289; b) J. Hahm, C. M. Lieber, *Nano Lett.* **2004**, *4*, 51.

[5] a) F. Hideo, M. Takashi, K. Seigo, Y. Hiroshi, L. Junji, *Appl. Phys. Lett.* **2001**, *78*, 2560; b) Y. K. Choi, J. Zhu, J. Grunes, J. Bokor, G. A. Somorjai, *J. Phys. Chem. B* **2003**, *107*, 3340; c) K. M. Chang, K. S. You, J. H. Lin, J. T. Sheu, *J. Electrochem. Soc.* **2004**, *151*, G679; d) R. Juhasz, N. Elfstrom, J. Linnros, *Nano Lett.* **2005**, *5*, 275; e) H. I. Liu, D. K. Biegelsen, F. A. Ponce, N. M. Johson, R. F. W. Pease, *Appl. Phys. Lett.* **1994**, *64*, 1383.

[6] a) J. Westwater, D. P. Gosain, S. Tomiya, S. Usui, H. Ruda, *J. Vac. Sci. Technol. B* **1997**, *15*, 554; b) Y. J. Zhang, Q. Zhang, N. L. Wang, Y. J. Yan, H. H. Zhou, J. Zhu, *J. Cryst. Growth* **2001**, *226*, 185; c) D. Gao, R. R. He, C. Carraro, R. T. Howe, P. D. Yang, R. Maboudian, *J. Am. Chem. Soc.* **2005**, *127*, 4574.

[7] A. I. Hochbaum, R. Fan, R. R. He, P. D. Yang, *Nano Lett.* **2005**, *5*, 457.

[8] a) P. Gorostiza, P. Allongue, R. Diaz, J. R. Morante, F. Sanz, *J. Phys. Chem. B* **2003**, *107*, 6454; b) J. S. Kim, H. Morita, J. D. Joo, T. Ohmi, *J. Electrochem. Soc.* **1997**, *144*, 3275; c) G. J. Norga, M. Platero, K. A. Black, A. J. Reddy, J. Michel, L. C. Kimerling, *J. Electrochem. Soc.* **1997**, *144*, 2801; d) G. Mattei, V. Valentini, *J. Am. Chem. Soc.* **2003**, *125*, 9608; e) D. A. Weinberger, S. G. Hong, C. A. Mirkin, B. W. Wessels, T. B. Higgins, *Adv. Mater.* **2000**, *12*, 1600; f) K. Q. Peng, J. Zhu, *Electrochim. Acta* **2004**, *49*, 2563.

[9] a) V. Lehmana, U. Gosele, *Adv. Mater.* **1992**, *4*, 114; b) P. Kleimann, X. Badel, J. Linnros, *Appl. Phys. Lett.* **2005**, *86*, 183108; c) Y. H. Zhang, X. J. Li, L. Zheng, Q. W. Chen, *Phys. Rev. Lett.* **1998**, *81*, 1710; d) K. Q. Peng, Y. Wu, H. Fang, X. Y. Zhong, Y. Xu, J. Zhu, *Angew. Chem.* **2005**, *117*, 2797; *Angew. Chem. Int. Ed.* **2005**, *44*, 2737; e) K. Q. Peng, J. J. Hu, Y. J. Yan, Y. Wu, H. Fang, Y. Xu, S. T. Lee, J. Zhu, *Adv. Funct. Mater.* **2006**, *16*, 387.

[10] a) K. Q. Peng, Y. J. Yan, S. P. Gao, J. Zhu, *Adv. Mater.* **2002**, *14*, 1164; b) K. Q. Peng, J. Zhu, *J. Electroanal. Chem.* **2003**, *558*, 35; c) K. Q. Peng, Y. J. Yan, S. P. Gao, J. Zhu, *Adv. Funct. Mater.* **2003**, *13*, 127.

[11] a) W. S. Shi, H. Y. Peng, Y. F. Zheng, N. Wang, N. G. Shang, Z. W. Pan, C. S. Lee, S. T. Lee, *Adv. Mater.* **2000**, *12*, 1343; b) Y. F. Zhang, Y. H. Tang, C. Lam, N. Wang, C. S. Lee, I. Bello, S. T. Lee, *J. Cryst. Growth* **2000**, *212*, 115.

[12] a) A. M. Morales, C. M. Lieber, *Science* **1998**, *279*, 208; b) M. K. Sunkara, S. Sharma, R. Miranda, G. Lian, E. C. Dickey, *Appl. Phys. Lett.* **2001**, *79*, 1546.

[13] a) H. Morinaga, M. Suyama, T. Ohmi, *J. Electrochem. Soc.* **1994**, *141*, 2834; b) J. S. Kim, H. Morita, J. D. Joo, T. Ohmi, *J. Electrochem. Soc.* **1997**, *144*, 3275; c) N. Mitsugi, K. Nagai, *J. Electrochem. Soc.* **2004**, *151*, G302.

[14] K. Tsujino, M. Matsumura, *Adv. Mater.* **2005**, *17*, 1045.

[15] L. T. Canham, *Appl. Phys. Lett.* **1991**, *57*, 1046.

Received: January 9, 2006
Revised: April 21, 2006
Published online: July 26, 2006

 © 2006 Wiley-VCH Verlag GmbH & Co. KGaA, Weinheim